PROCEEDINGS OF THE ROYAL SOCIETY A

rspa.royalsocietypublishing.org

Research

Cite this article: Noselli G, DeSimone A. 2014 A robotic crawler exploiting directional frictional interactions: experiments, numerics and derivation of a reduced model. *Proc. R. Soc. A* **470**: 20140333.
http://dx.doi.org/10.1098/rspa.2014.0333

Received: 25 April 2014
Accepted: 29 August 2014

Subject Areas:
mechanics, biomechanics

Keywords:
crawling motility, directional interactions, directional surfaces, breathing-like deformations, scallop theorem

Author for correspondence:
Giovanni Noselli
e-mail: giovanni.noselli@sissa.it

Electronic supplementary material is available at http://dx.doi.org/10.1098/rspa.2014.0333 or via http://rspa.royalsocietypublishing.org.

Royal Society Publishing

A robotic crawler exploiting directional frictional interactions: experiments, numerics and derivation of a reduced model

Giovanni Noselli[1] and Antonio DeSimone[1,2]

[1]SISSA-International School for Advanced Studies, via Bonomea 265, 34136 Trieste, Italy
[2]GSSI-Gran Sasso Science Institute, viale Francesco Crispi 7, 67100 L'Aquila, Italy

We present experimental and numerical results for a model crawler which is able to extract net positional changes from reciprocal shape changes, i.e. 'breathing-like' deformations, thanks to directional, frictional interactions with a textured solid substrate, mediated by flexible inclined feet. We also present a simple reduced model that captures the essential features of the kinematics and energetics of the gait, and compare its predictions with the results from experiments and from numerical simulations.

1. Introduction

The mechanics of locomotion at small scales is receiving increasing attention in the recent literature. This is due both to the intrinsic interest in the detailed understanding of the locomotion strategies of small biological organisms [1,2] and in the interest in reproducing them in artificial, bioinspired artefacts [3,4]. Depending on whether self-propulsion forces arise from the mechanical interactions of the locomotor with a surrounding fluid, or with a solid substrate, motility occurs by either swimming or crawling, and these are the main motility modes at microscopic scales [5].

The study of crawling at microscopic scales is often motivated by the interest in cell motility and spreading [6,7]. In another stream of research, limbless locomotion has attracted interest as a new paradigm for robotic locomotion in very rough and complex environments or on uneven terrains [3,8,9]. Besides the engineering

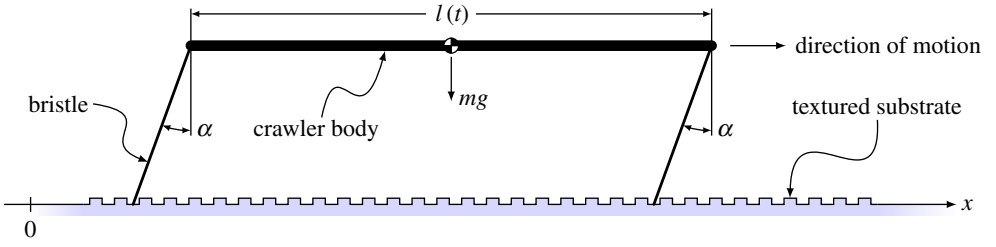

Figure 1. A sketch of the model *bristle-crawler* analysed in this study. The system comprises an initially horizontal body of current length $l(t)$ and mass m, interacting with a groove-textured substrate by means of two inclined, flexible bristles. Owing to the inclination of the elastic bristles, the frictional interaction arising at the crawler/substrate interface is directional in nature. Note that the system is externally subject only to vertical gravitational loads. (Online version in colour.)

interest in view of the possible technological applications (rescue robotics, industrial inspection, medical endoscopy), the comparison of the behaviour of biological organisms with robotic replicas is particularly fruitful in that it promotes a synthetic, functionalist view of biological and bioinspired motility, in which the essential necessary ingredients can be identified, and the way they interact can be studied in detail [10–12].

One of the themes that emerges naturally from the studies above is the identification of the mechanisms of minimal complexity that are able to produce non-zero net displacements by exploiting periodic shape changes. In swimming micromotility, when the size of the swimmer is sufficiently small and the induced flows are characterized by low Reynolds numbers (*Re*), net displacements can be obtained only through non-reciprocal shape changes. This fact is known as the Scallop theorem in the microswimming literature [13]. A geometrical view emphasizing how the key to self-propulsion for low *Re* swimmers resides in performing closed loops in the space of shapes is discussed in [14–19], pursuing ideas pioneered in [20].

In fact, we have shown in recent work that many ideas emerged in the context of low *Re* swimmers can be useful also in the crawling setting [21–23]. A question that is particularly intriguing is whether, by exploiting sufficiently nonlinear interactions with a substrate one may *beat* the Scallop theorem, and achieve non-zero net displacement for a locomotor that can only change shape in a reciprocal manner, through breathing-like deformations. Such deformations are represented by an open curve in the space of shapes, travelled forward and backward. While such shape changes produce zero net displacements in low *Re* swimming, this is no longer the case for crawlers on solid substrates, provided that the frictional interactions with the substrate are 'directional' [24]. By this, we mean interactions such that the force–velocity relation is not odd. Surface directionality is common in nature, and in fact, it provides specific functions for the survival of many species in the plant and animal kingdoms, see for instance the review on bioinspired textured surfaces in reference [25]. A detailed theoretical study of the motion of model crawlers exploiting distributed, directional interactions is contained in reference [26], whereas the first example of a self-oscillating gel, driven by the Belouzov–Zhabotinsky reaction and crawling on a textured surface, is reported in earlier studies [27–29].

The goal of this paper was to show how a crawler exploiting directional interactions can be realized in practice, and how a simple model of the type studied in reference [26] can be adequate to analyse its behaviour, resolving in a satisfactory way both the kinematics of the gait and its energetics.

In this study, we shall consider the prototypical bristle-crawler shown in figure 1. Bristle-robots have already been used in the past as model systems [21,30]. The system comprises an initially horizontal segment of current length $l(t)$ and mass m, interacting with a groove-textured surface by means of two inclined, flexible bristles. The inclination of the bristles by the angle α gives rise to directional frictional interactions, such that reciprocal length changes of the crawler body lead to its advancement on the substrate. Ours is only one of the possible choices to produce

an effective frictional interaction with a force–velocity relation that is not odd. For example, one could texture the crawler instead of the substrate, and many alternative designs can be pursued based, for instance, on the bioinspired surfaces reviewed in reference [25].

In the following, we explore the crawler's motility both via direct experimentation and via finite-element computations. These analyses will lead to the definition of a simplified, one-dimensional model capable of resolving both the kinematics and the energetics of the system being analysed.

The focus of our paper is on the net displacements that can be extracted from the most elementary form of cyclic shape changes, namely reciprocal breathing-like deformations. Previous studies in the literature had mostly focused on peristaltic locomotion, where shape changes consist in travelling waves of extension or contraction [2,8,9], a mechanism requiring a much more sophisticated level of spatio-temporal coordination. However, we share with these studies the interest in clarifying the basic aspects in the modelling of frictional interactions with a substrate, a necessary preliminary step on the way to obtain reliable models for the design of self-propelled microrobots, bioinspired by the crawling motility of invertebrate organisms.

2. Experimental analysis of the *bristle-crawler*

Here, we begin the analysis of the *bristle-crawler* sketched in figure 1 by direct experimentation. The experimental setting employed in the study is shown in figure 2. It comprises a prototype of the robotic crawler, positioned on a groove-textured substrate and actuated by means of a shape–memory–alloy (SMA) spring, an array of three fans, employed to enhance the convective cooling of the actuating coil and the control/acquisition electronics.

All the components of the crawler's body were obtained using a EGX-600 CNC machine from Roland Corporation to engrave a 10 mm thick plate of transparent PMMA, whereas the supports for the flexible bristles were realized with a 3DS Project 3510 HD printer to provide an inclination of $\alpha = \pi/4$.[1] Similarly, a mould was three-dimensionally printed for the preparation of the flexible bristles with a Shore A 40 silicone rubber. A tapered shape was chosen for the bristles in order to ensure interlocking between their tips and the substrate grooves: the cross section of 30×3 mm at the bristle clamp linearly decreases to a cross section of 30×0.5 mm at the bristle tip, for an overall length of 5 mm. Specifically, see figure 2*b*,*c*, the prototype crawler, of overall mass 55 g and distance between the bristles 100 mm, was designed symmetric about the anterior–posterior vertical plane, and each of its sides simply comprises two segments sliding side by side to provide a maximum shortening $\tilde{s} = 20$ mm via the resistive heating of the SMA actuator. The preparation of the textured substrate also required the use of the CNC machine to engrave evenly spaced rectangular symmetric grooves 1 mm wide and 0.25 mm deep in a 3 mm thick plate of white PMMA.

For the actuation of the robotic crawler, an SMA tension spring was chosen as a lightweight and compact solution. This was purchased from Jameco Electronics and comprises 20 active coils with an outer diameter of 6 mm and a wire diameter of 0.75 mm. Its connection to the crawler body was achieved by means of two ending hooks. The shortening mechanism of the crawler was designed in such a way that its contraction implies the extension of two rubber bands, which act as antagonist, restoring elements for the SMA spring.

Each trial was carried out at room temperature (22°C) and with the three fans (from Jamicon Electronics, model JF0925-1UR) running at 3500 rpm. The displacement at the left and right ends of the crawler was measured with two triangulation, non-contact laser transducers (from Kyence, model IL-300) simultaneously sampled at a rate of $100\,\mathrm{S\,s^{-1}}$ via a cRIO-9082 from National Instruments endowed with a NI-9215 AI module. This allowed for the determination of the crawler position, namely the displacement of its right-hand side $\Delta(t)$, as a function of its shortening $s(t)$. The acquired shortening $s(t)$ was also exploited as feedback for a closed-loop

[1]In this study, we focus on the significance of directional interactions to crawling motility; a detailed analysis of the sensitivity of crawling performance to the number and inclination of the bristles is currently being performed and will be the subject of a forthcoming paper.

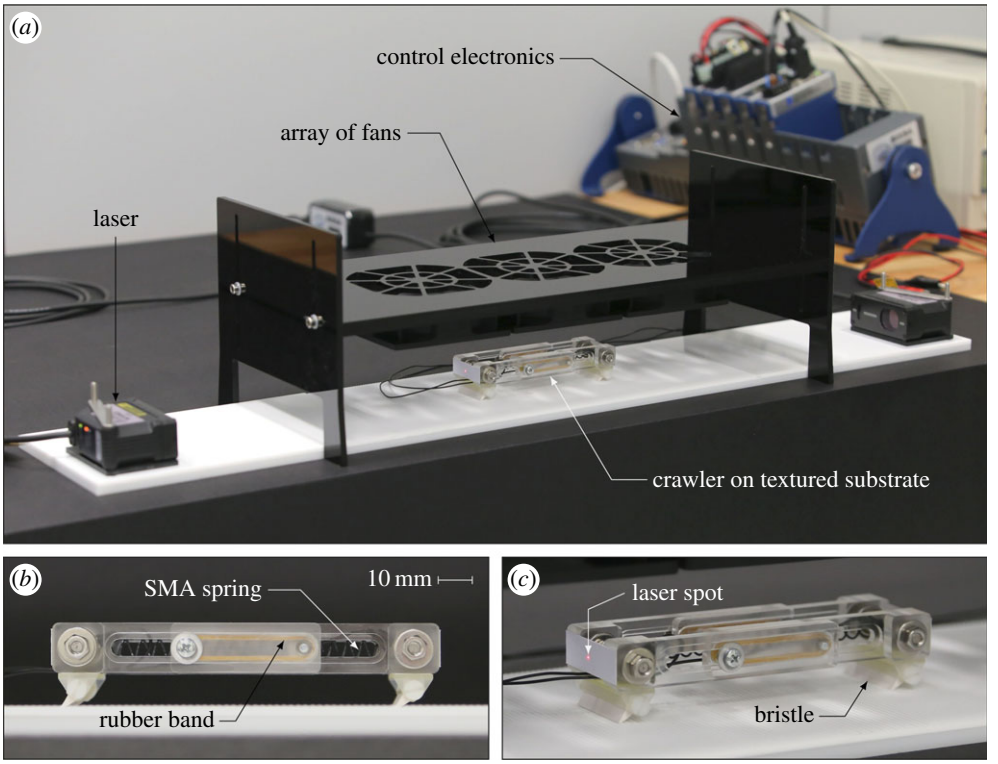

Figure 2. The practical realization of the *bristle-crawler* analysed in this study. A global view of the experimental setting is reported in (*a*), whereas (*b*) and (*c*) are closer side views of the prototype crawler. Note the SMA spring employed as actuator and the elastic rubber bands acting as antagonist, restoring elements. The length of the crawler, taken as the distance between the two bristles, is of 100 mm for an overall mass of 55 g, whereas the available shortening provided by the sliding mechanism is $\tilde{s} = 20$ mm. (Online version in colour.)

control implemented on the FPGA of the cRIO-9082. In fact, at the beginning of each test an electric current of 3.5 A was delivered to the SMA actuator through two tiny and flexible cables connected to a home-made amplifier, operating in commutation mode and controlled by a NI-9472 DO module, while monitoring the crawler shortening. When the shortening $s(t)$ attained the peak value of 20 mm, the delivery of electric current was stopped by the control loop, allowing the robotic crawler to re-extend, thanks to the convective cooling provided by the fans. Again, the shortening $s(t)$ was monitored, and no current was delivered to the actuator until the crawler returned to its original length. This cycle was repeated at least five times during each trial, and any individual stretching cycle approximately required a time of 20 s.

The experimental analysis of the *bristle-crawler* allowed for the precise determination of its motile behaviour. During each trial we observed, as expected, a rightwards motion of the system, with the two bristles sliding at different times in the direction of less resistance (i.e. 'along the grain' of the texture). This is also clearly visible from the movie provided in the electronic supplementary material (part I), which was taken with a digital camera EOS 6D from Canon, equipped with a EF 24–105 mm 1 : 4 L IS USM objective. In particular, the movie in the electronic supplementary material shows the results of two distinct trials, carried out for an inclination α of the bristles of $\pi/4$ and 0, respectively. The second trial, with vertical bristles, was performed in order to experimentally prove the significance of the bristles inclination to directional interactions. In fact, for $\alpha = 0$, the motion of the system is characterized by almost symmetric oscillations about its middle point, so that no appreciable net advancement was observed during the test.

The crawler's advancement, namely the displacement $\Delta(t)$ of its right-hand side, is shown in figure 3 as a function of the shortening $s(t)$. In particular, five stretching cycles are reported and

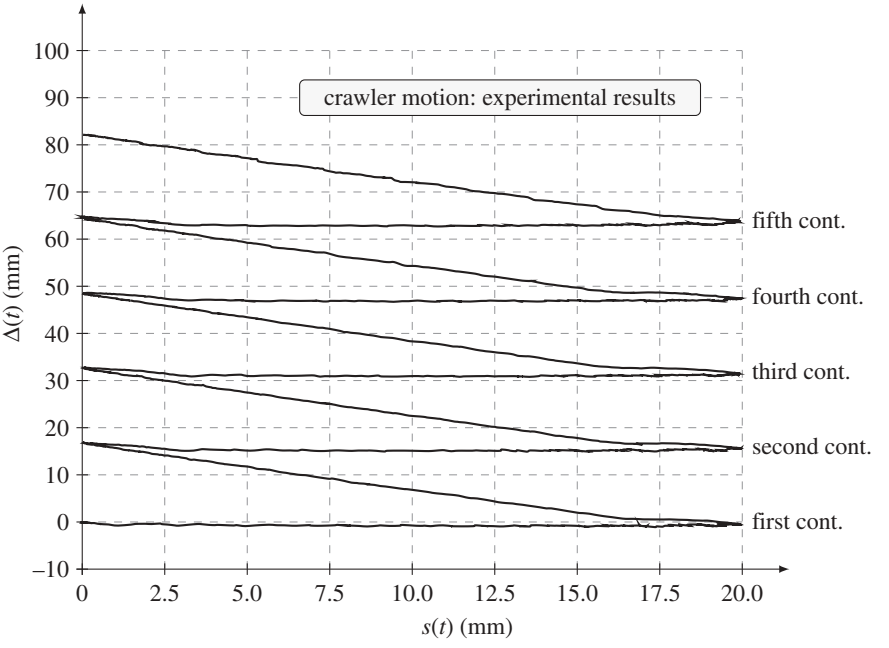

Figure 3. Displacement of the right-hand side of the crawler $\Delta(t)$ as a function of its shortening $0 \leq s(t) \leq \tilde{s}$. Five stretching cycles are reported, corresponding to a net advancement of approximately 82 mm. Note the changes in the slope of the diagram along the contraction and re-extension branches. These are due to the transitions between the *stick* and *slip* regimes of the two bristles. The advancement for each cycle is approximately 82% of the available shortening of 20 mm, a fact arising from the flexibility of the bristles.

these are highlighted in the figure. We note that the net advancement arising from the five cycles approximately equals 82 mm, and this is also the mean value measured from the experiments with a deviation of ± 1 mm. Thus, the advancement arising from each stretching cycle is always smaller than the maximum available shortening of 20 mm. The inspection of figure 3, together with the snapshots in figure 4, provides a rather clear explanation for that. In fact, during each cycle, the crawler experiences two distinct regimes, related to a *stick–slip* behaviour of the bristles. During contraction, the two bristles initially deform elastically and their tips are at rest (the two bristles *stick*). Upon attainment of a critical shortening, the left bristle slides rightwards, whereas the other one keeps its position (*slip* of the left bristle and *stick* of the right one). Likewise, during re-extension, the two bristles are first elastically deformed in the opposite direction with their tips at rest (*stick* of the two bristles), and then the right bristle slides rightwards, whereas the other one keeps again its position (*stick* of the left bristle and *slip* of the right one). It turns out that the flexibility of the two bristles which mediate the interaction with the substrate significantly affects the crawler motility. Indeed, a part of the available shortening is spent in each cycle, both during contraction and re-extension, to bend elastically the bristles before sliding of their tips can take place.

The two regimes experienced by the crawler can be easily detected from the results of figure 3, where the transition between *stick* and *slip* of the bristles typically corresponds to an evident change in the slope of the diagram along the contraction and re-extension branches. This is less visible during the first contraction due to the fact that, at the beginning of the test, the two bristles are almost unloaded and subject only to vertical, gravitational forces, whereas, at the beginning of all the following branches, the two bristles are always in a state of horizontal pre-loading.

Snapshots of the crawler position during a typical test are reported in figure 4. Specifically, five stretching cycles are shown for direct comparison with figure 3 and, for each cycle, the initial configuration of the crawler is reported together with the two configurations after a contraction

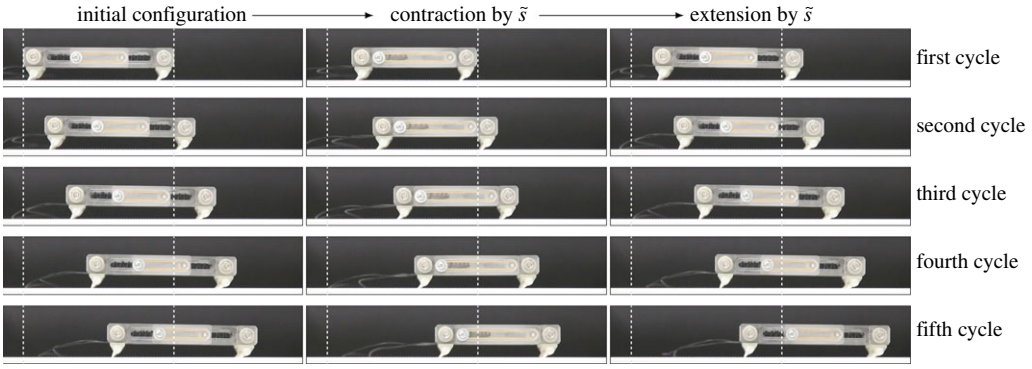

Figure 4. Snapshots of the robotic crawler performing five stretching cycles. For each cycle, the initial configuration of the crawler is reported together with the two configurations after a contraction by $\tilde{s}$ and after the re-extension to the original length. Note that vertical, dashed lines are drawn to highlight the displacement of the left and right extremities of the crawler's body. The last picture of each cycle is repeated for clarity as the first one of the following cycle. (Online version in colour.)

by $\tilde{s}$ and after the re-extension to the original length. Note that vertical, dashed lines are drawn to highlight the displacement of the left and right extremities of the crawler's body, whereas the last picture of each cycle is repeated for clarity as the first one of the following cycle. Inspection of the deformed shapes of figure 4 sheds light on the motile behaviour of the robotic crawler: the net advancement is achieved by a sequence of *stick–slip* events for the flexible bristles, with horizontal displacements much larger than the vertical ones. In the following, see §4, we shall exploit these observations for the definition of an effective, one-dimensional model for crawling motility.

3. Finite-element computations

The experimental analysis of the *bristle-crawler* allowed for the determination of the key mechanisms behind its kinematics. We extend now our study via numerical computations, by setting a finite-element model capable of reproducing all the features of the crawler's motility that were observed during direct experimentation. We will use the results from the finite-element computations to quantify the forces and the energetics of the model system under investigation.

The commercial software ABAQUS Standard 6.13-2 was employed to run the analyses. Specifically, the crawler body was modelled as a horizontal connector of type CONN2D2 with initial length of 100 mm, whereas the elastic bristles were modelled with two-nodes B21 beam elements. Their tapered shape was taken into account and, to this purpose, each bristle was discretized by means of 100 finite-elements of variable cross section for an overall length of 5 mm. With respect to the material properties, a Young's modulus of 1.1 MPa, a Poisson's ratio of 0.45 and a mass density of $1.3\,\mathrm{g\,cm^{-3}}$ were chosen for the Shore A 40 silicone rubber, and viscous dissipation was accounted for by means of Rayleigh mass-proportional damping corresponding to a damping ratio of 0.15 at the first resonant frequency. The flexible bristles were fixed to the crawler's body by means of rigid, vertical links ending at the extremities of the horizontal connector, where two point masses of 27.5 g each were also attached to account for the overall inertia of the system (these are depicted as black spots in figure 6, where also the discretization described above can be recognized). The textured substrate was introduced in the model as an analytical rigid surface, resembling the precise geometry employed in the experiments, and Coulomb dry friction was assumed at the contact between the bristles and the rigid surface. Remarkable agreement between the numerical predictions and the experimental results was obtained for a friction coefficient of 0.65, consistently with the properties of the two materials in contact.

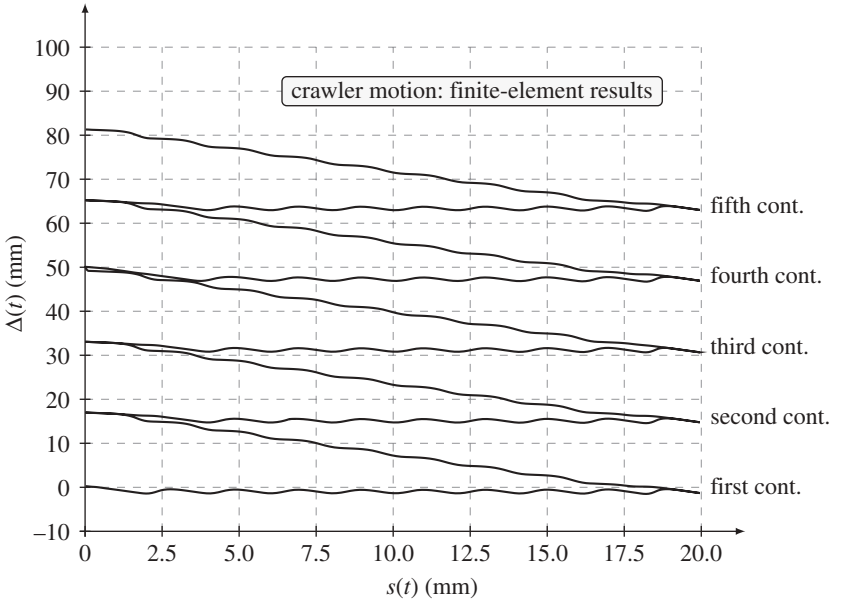

Figure 5. Displacement of the right end of the crawler $\Delta(t)$ as a function of its shortening $0 \leq s(t) \leq \tilde{s}$. Five stretching cycles are reported, corresponding to a net advancement in line with the experimental measures (figure 3). Note the small-amplitude oscillations in the advancement arising from the elasticity of the bristles and the discrete nature of the interaction between the bristles and the substrate. Just as in the experiments, the advancement in each cycle is smaller than the available shortening of 20 mm, a fact arising from the flexibility of the bristles.

Each finite-element analysis comprised two steps and both were run in a nonlinear, large deformation framework taking into account inertial effects. The crawler, positioned on the textured surface, was first subjected to vertical gravitational loads (step 1), and then periodic shape changes were prescribed to the horizontal connector by means of a user subroutine DISP (step 2), with imposed shortening $s(t) = \tilde{s}\sin^2(\pi t/T)$, with a peak value $\tilde{s} = 20$ mm and a period $T = 20$ s.

As a first numerical result, we show in figure 5 the crawler's advancement $\Delta(t)$ as a function of its shortening $s(t)$ for an inclination of the bristles $\alpha = \pi/4$. In particular, five stretching cycles are reported, as highlighted in figure 5, such that a direct comparison with the experimental results of figure 3 is feasible. A remarkable agreement was found for the set of material parameters reported above and, in fact, the finite-element model well captures all the features of the crawler gait. Small-amplitude oscillations in the advancement $\Delta(t)$ are visible along the branches of the graph, and these arise from the elastic deformability of the bristles loaded by oscillating forces owing to the discrete nature of the interaction between bristle tips and textured surface.

The finite-element analyses were run accounting for the inertia of the system, but it seems reasonable, both from the experiments and the numerical computations, to conclude that for the prescribed time history of shape changes the crawler's gait falls within the quasi-static regime. We shall exploit this observation in §4.

Deformed shapes of the crawler are reported in figure 6, and these were extracted from the numerical simulations. Again, five stretching cycles are reported, and remarkable agreement is found with the experimental snapshots of figure 4, a fact that further validates the adequacy of the proposed model to capture the gait of the crawler. The crawler's motion is also reported in the movie provided in the electronic supplementary material (part II), which shows the results from two distinct computations as obtained for an inclination of the bristles of $\alpha = \pi/4$ and $\alpha = 0$.

The computational results reported in figures 5 and 6 mainly concern the kinematics of the system under investigation. However, in this study, we are also interested in exploring the energy

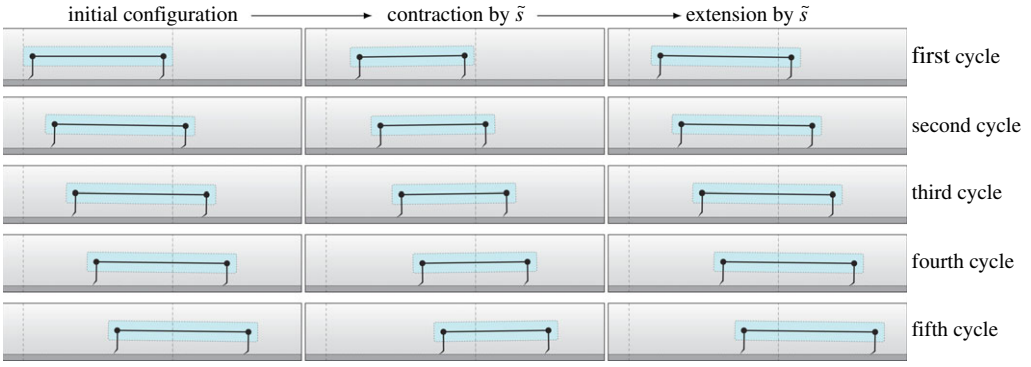

Figure 6. Deformed shapes of the robotic crawler performing five stretching cycles. For each cycle, the initial configuration of the crawler is reported together with the two configurations after a contraction by $\tilde{s}$ and after the re-extension to the original length. Note that vertical, dashed lines are drawn to highlight the displacement of the left- and right-hand side of the crawler's body. The last picture of each cycle is repeated for clarity as the first one of the following cycle. (Online version in colour.)

cost related to crawling motility, and this is feasible by computing the forces experienced by the connector while performing periodic shape changes. To this aim, results were extracted from the numerical computations and are summarized in figure 7 for the interesting case of $\alpha = \pi/4$. In particular, we report in figure 7*a* the time history of the force $F_c(t)$ experienced by the axial connector during five stretching cycles, corresponding to an overall time of 100 s. Likewise, the work $W_c(t)$ expended by the connector during those stretching cycles is shown in figure 7*b*. The inspection of these results reveals the oscillatory, irregular nature of the frictional interaction arising at the crawler/substrate interface, and allows for a precise evaluation of the energetics associated with crawling motility in the context of directional interactions. As anticipated, we shall employ the experimental observations on the crawler gait and the computational results related to the energetics of crawling in the formulation of an effective, one-dimensional model.

4. A one-dimensional model for the *bristle-crawler*

In the previous sections, locomotion of the *bristle-crawler* has been extensively investigated both by means of experiments on a small-scale prototype and via detailed finite-element computations. The analysis of those results, in particular of the deformed shapes shown in figures 4 and 6, reveals that the kinematics of the system essentially comprises horizontal displacements. In fact, the crawler shortening $\tilde{s}$ much exceeds the vertical displacements, which only arise from the inflection of the bristles and from their adaptation to the irregularities of the substrate.

In this study, directional interactions have been achieved through the sliding of inclined bristles on a groove-textured substrate. The question arises whether such interactions can be suitably modelled by means of an effective force–velocity law. In view of the results discussed in the previous sections, a natural starting point is the following one-dimensional law:

$$F_i(t) = \begin{cases} F_n & \text{if } \dot{x}_i(t) < 0, \\ \tilde{F} \in [-F_p, F_n] & \text{if } \dot{x}_i(t) = 0, \\ -F_p & \text{if } \dot{x}_i(t) > 0, \end{cases} \tag{4.1}$$

where $F_i(t)$ is the horizontal force acting on the ith bristle tip, function of its sliding velocity $\dot{x}_i(t)$ and of the non-negative parameters F_p and F_n, see also figure 8. In equation (4.1), the subscript $i = \{1, 2\}$, whereas the two parameters F_p and F_n correspond to the average frictional forces acting on the bristle while sliding along the grain or against it, respectively. Note that, owing to the inclination of the two bristles by the angle α, F_n always exceeds F_p.

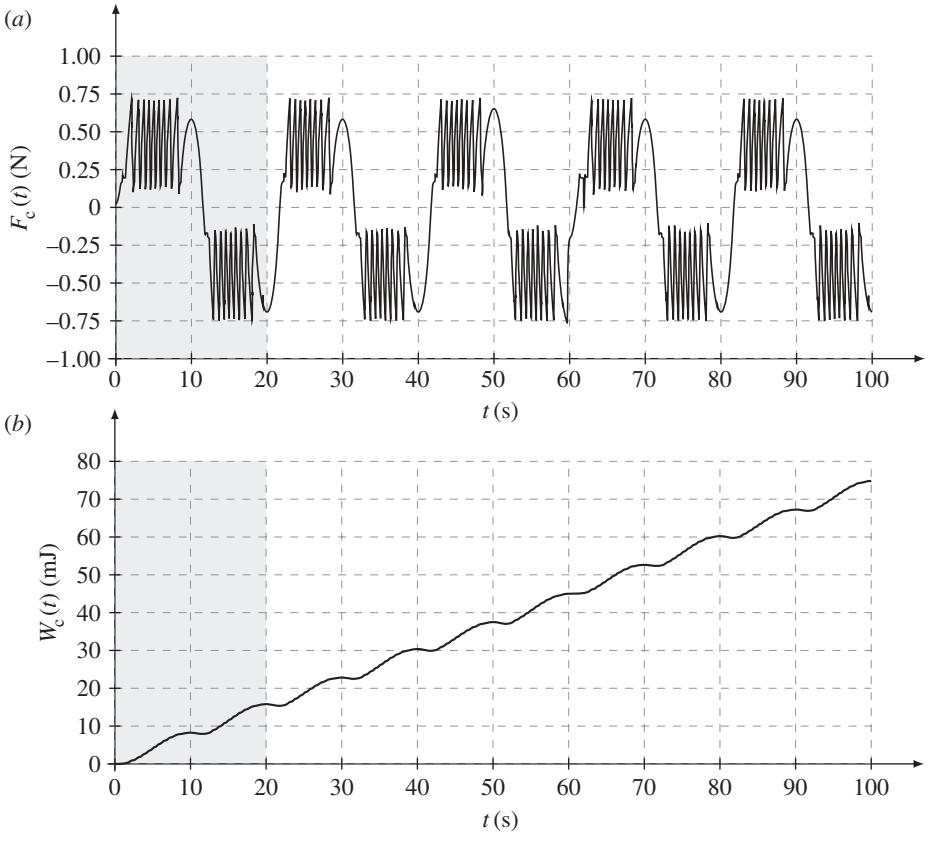

Figure 7. Computed force $F_c(t)$ acting on the horizontal connector (*a*) and work performed by the connector $W_c(t)$ during cyclic shape changes (*b*). Note that five cycles are reported, corresponding to an overall time of 100 s for the analysis. The time interval for the first stretching cycle is highlighted.

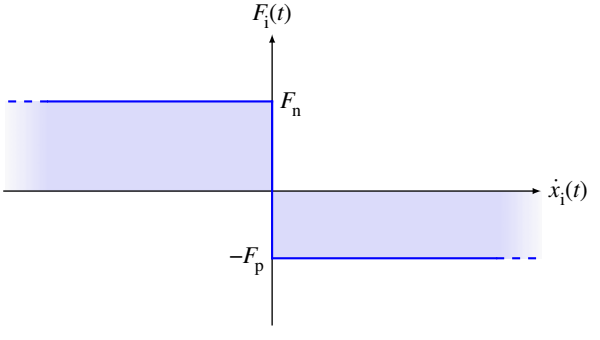

Figure 8. A representation of the directional force–velocity law employed in this study. Owing to the inclination of the bristles $F_n > F_p$, where the higher friction corresponds to negative sliding velocities. (Online version in colour.)

It turns out that a simplified, one-dimensional model can be set for the bristle-crawler. This is shown in figure 9, where the crawler's body is depicted with a horizontal segment of current length $l(t)$. The two bristles are modelled as vertical, rigid links and their compliance is accounted for by means of two linear springs of stiffness k and unloaded length δ^0, so that the tips of the bristles (denoted by tiny solid triangles) are given an initial horizontal offset with respect to the

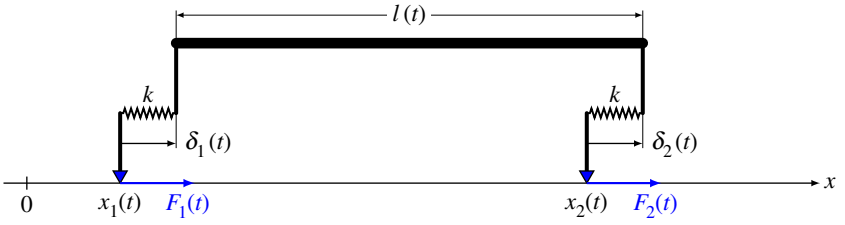

Figure 9. A sketch of the one-dimensional model for the *bristle-crawler*. The model accounts only for horizontal displacement, and the two points $x_1(t)$ and $x_2(t)$ are subjected to frictional, horizontal forces as given by the law of equation (4.1), see also figure 8. (Online version in colour.)

crawler extremities. Frictional, directional interactions between the substrate and the bristles are described by equation (4.1).

We extend now our approach to *quasi-static crawling* [21–23,26] by considering T-periodic, reciprocal shape changes of the system shown in figure 9, such that its length first monotonically decreases from the initial value of L to $L-\tilde{s}$, and then monotonically increases from $L-\tilde{s}$ to L. At any instant t, the configuration of the system is known upon determination of the two coordinates $x_i(t)$ and of the two lengths $\delta_i(t)$, with $i=\{1,2\}$. The compatibility of the displacements requires that

$$x_2(t)+\delta_2(t)=x_1(t)+\delta_1(t)+l(t), \tag{4.2}$$

whereas the balance of the horizontal forces acting on the crawler simply reads

$$F_1(t)+F_2(t)=0. \tag{4.3}$$

Because the forces $F_i(t)$ are transmitted to the crawler body by the elastic springs, we can set

$$F_i(t)=-k[\delta_i(t)-\delta^0], \tag{4.4}$$

and force balance provides the following relation between their lengths

$$\delta_2(t)=2\delta^0-\delta_1(t). \tag{4.5}$$

The frictional law employed in this study requires the forces $F_i(t)$ to attain a constant yield value in order for sliding to occur, such that the problem under consideration possesses similarities with the constitutive theory for elastic, ideally plastic solids [31] and can be conveniently approached in rate form. A similar approach has also been used to model the motion of capillary drops on rough substrates, see [32,33]. Direct substitution of equation (4.5) into equation (4.2) and time differentiation yields

$$\dot{x}_2(t)=\dot{x}_1(t)+2\dot{\delta}_1(t)+\dot{l}(t), \tag{4.6}$$

an equation that can be integrated by splitting the stretching cycle in distinct stages. Furthermore, note that, in view of the restriction $F_n>F_p$, force balance dictates sliding to occur by a positive velocity and at one bristle tip at most, so that, while sliding, the crawler is subjected to two balanced forces of modulus F_p.

(a) Stage a: $t\in[0,t_a)$ and $|F_i(t)|<F_p$.

We assume the crawler to be unloaded in its initial configuration, where $F_i(0)=0$ and $\delta_i(0)=\delta^0$. We further take $x_1(0)=0$ and $x_2(0)=L$ as initial conditions. Hence, by setting $\dot{x}_1(t)=\dot{x}_2(t)=0$ in

equation (4.6). we immediately obtain

$$\dot{\delta}_1(t) = -\frac{\dot{l}(t)}{2}, \tag{4.7}$$

which, upon time integration and substitution into equation (4.4), provides the expressions of the two balanced forces as

$$F_1(t) = -F_2(t) = -\frac{k[L - l(t)]}{2} = -\frac{ks(t)}{2}, \tag{4.8}$$

where the shortening at time t has been introduced as $s(t) = L - l(t)$. Note that $F_1 < 0$ and $F_2 > 0$, so that equation (4.8) holds as long as $F_1 > -F_p$. Therefore, at time $t = t_a$ the onset of sliding takes place at the tip of the left bristle for

$$s(t_a) = \frac{2F_p}{k}. \tag{4.9}$$

Upon definition of $\Delta(t) = x_2(t) + \delta_2(t) - L - \delta^0$, we obtain from the equations above the expression for the displacement of the right-hand side of the crawler, namely

$$\Delta_a^1(t) = -\frac{s(t)}{2} \geq -\frac{F_p}{k}, \tag{4.10}$$

with the superscript '1' denoting the first stretching cycle. It is worth noting that if $\tilde{s} < 2F_p/k$ sliding cannot take place, so that, during re-extension, the system essentially recovers its original configuration by elastically unloading the two springs.

(b) Stage b: $t \in [t_a, t_b)$ and $|F_i(t)| = F_p$.

At the beginning of this second stage $s(t_a) = 2F_p/k$, while the crawler is subjected to balanced forces of modulus F_p. Hence, by further increasing the shortening up to $\tilde{s}$, the left bristle slides rightwards, whereas $\dot{x}_2(t) = \dot{\delta}_1(t) = \dot{\delta}_2(t) = 0$. Consequently, the displacement of the right-hand side remains unchanged and reads as

$$\Delta_b^1(t) = \Delta_a^1(t_a) = -\frac{F_p}{k}. \tag{4.11}$$

(c) Stage c: $t \in [t_b, t_c)$ and $|F_i(t)| < F_p$.

Upon decreasing the shortening $s(t)$, the two elastic springs unload and the moduli of the forces also, i.e. $|F_i(t)|$, decrease. Therefore, we can again set $\dot{x}_1(t) = \dot{x}_2(t) = 0$ in equation (4.6), so that, by time integration of equation (4.7) and substitution into equation (4.4), we obtain the expressions of the forces as

$$F_1(t) = -F_2(t) = -\frac{k[s(t) - \tilde{s}]}{2} - F_p. \tag{4.12}$$

As $s(t)$ decreases, the two forces first vanish, and then invert their signs. For sufficiently small values of $s(t)$, $F_1 > 0$ and $F_2 < 0$, so that equation (4.12) holds as long as $F_2 > -F_p$. Hence, at time $t = t_c$, sliding takes place at the tip of the right bristle for

$$s(t_c) = \tilde{s} - \frac{4F_p}{k}. \tag{4.13}$$

By making use of the equations above and of the definition of $\Delta(t)$, we easily obtain the expression for the displacement of the right end of the crawler as

$$\Delta_c^1(t) = -\frac{F_p}{k} + \frac{\tilde{s} - s(t)}{2} \leq \frac{F_p}{k}. \tag{4.14}$$

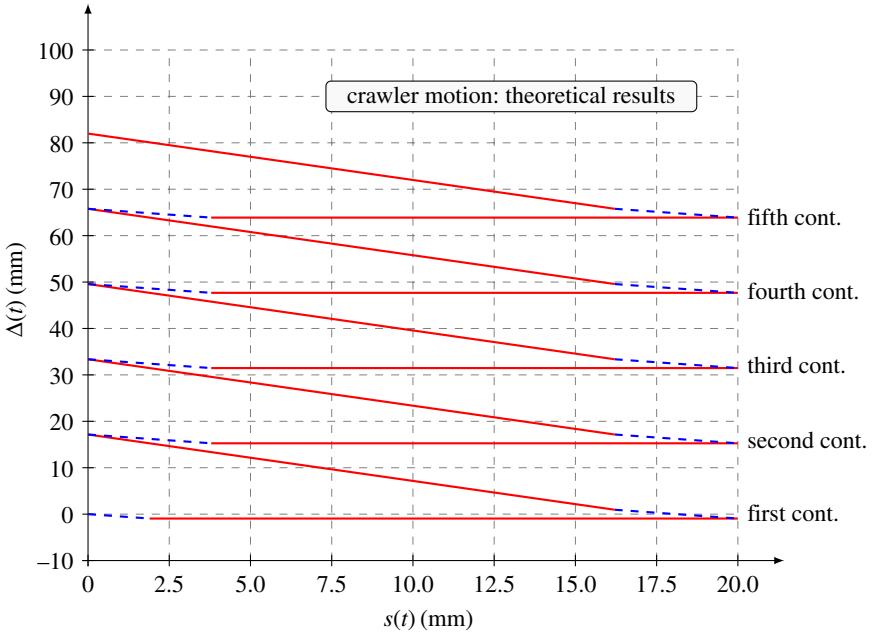

Figure 10. Displacement of the right end of the crawler $\Delta(t)$ as a function of its shortening $0 \leq s(t) \leq \tilde{s}$. Note that five stretching cycles are reported, with dashed and solid segments denoting the two regimes of stick and slip for the bristles, respectively. (Online version in colour.)

(d) Stage d: $t \in [t_c, T]$ and $|F_i(t)| = F_p$.

At the beginning of the last stage $s(t_c) = \tilde{s} - 4F_p/k$, while the crawler is again subject to balanced forces of modulus F_p. Hence, by decreasing the shortening to zero, the right bristle slides rightwards. By setting $\dot{x}_1(t) = \dot{\delta}_1(t) = \dot{\delta}_2(t) = 0$ into equation (4.6), we obtain

$$\dot{x}_2(t) = \dot{l}(t), \tag{4.15}$$

which, upon time integration, provides the displacement of the right-hand side as

$$\Delta_d^1(t) = \tilde{s} - s(t) - \frac{3F_p}{k}. \tag{4.16}$$

The net advancement achieved during the first stretching cycle can be derived from equation (4.16) by setting $s(T) = s(0) = 0$, leading to

$$\Delta_{net}^1 = \tilde{s} - \frac{3F_p}{k}. \tag{4.17}$$

The result of equation (4.17) concludes the analysis of the first stretching cycle and sheds light on the effect of the bristle stiffness on the crawler motility. In fact, as already observed through direct experimentation and numerical computations, the net advancement is less than the available shortening, and their difference, i.e. $-3F_p/k$, arises from the flexibility of the bristles. It is also worth noting that, owing to the assumption of *quasi-static crawling*, the results above do not depend on the precise time history of the shortening $s(t)$, provided the contraction and re-extension of the crawler are monotonic in time.

Subsequent stretching cycles can be similarly analysed, the only difference arising from the fact that, while at the beginning of the first cycle the crawler is unloaded, i.e. $F_i(0) = 0$, this is not the case of the following cycles and, in fact, $|F_i(T)| = F_p$.

Denoting by $n \geq 2$ the stretching cycle number, the expression for the displacement at the right-hand side of the crawler follows as

$$\Delta^n(t) = \begin{cases} -\dfrac{s(t)}{2} + \Delta^1_{\text{net}} + \left(\tilde{s} - \dfrac{4F_{\text{p}}}{k}\right)(n-2) & \text{for } 0 \leq s(t) < \dfrac{4F_{\text{p}}}{k}, \\ -\dfrac{2F_{\text{p}}}{k} + \Delta^1_{\text{net}} + \left(\tilde{s} - \dfrac{4F_{\text{p}}}{k}\right)(n-2) & \text{for } \dfrac{4F_{\text{p}}}{k} \leq s(t) \leq \tilde{s}, \\ -\dfrac{2F_{\text{p}}}{k} + \dfrac{\tilde{s} - s(t)}{2} + \Delta^1_{\text{net}} + \left(\tilde{s} - \dfrac{4F_{\text{p}}}{k}\right)(n-2) & \text{for } \tilde{s} - \dfrac{4F_{\text{p}}}{k} < s(t) \leq \tilde{s}, \\ -\dfrac{4F_{\text{p}}}{k} + \tilde{s} - s(t) + \Delta^1_{\text{net}} + \left(\tilde{s} - \dfrac{4F_{\text{p}}}{k}\right)(n-2) & \text{for } 0 \leq s(t) \leq \tilde{s} - \dfrac{4F_{\text{p}}}{k}. \end{cases} \tag{4.18}$$

It turns out that the net advancement Δ^n_{net} for the subsequent stretching cycles is less than that of the first cycle by a factor F_{p}/k, namely

$$\Delta^n_{\text{net}} = \tilde{s} - \frac{4F_{\text{p}}}{k}, \tag{4.19}$$

the difference arising again from the state of pre-load of the bristles at the beginning and at the end of each cycle such that $n \geq 2$.

The crawler motion is shown in figure 10 in terms of the displacement at its end $\Delta(t)$ as a function of the shortening $0 \leq s(t) \leq \tilde{s}$. The results were obtained for $\tilde{s} = 20$ mm and assuming $F_{\text{p}}/k = 0.95$ mm, so that direct comparison is possible both with the results of figure 3 and of figure 5. Specifically, the value of F_{p}/k was computed on the basis of the experimental and computational results in order to obtain from equation (4.18) an advancement of 82 mm after five stretching cycles, i.e. for $n = 5$. Note that the results of figure 10 well capture the features of the crawler gait, such as the existence of the two regimes of stick and slip (and the related changes in the slope of the diagram along all the branches), shown as dashed and solid segments, respectively.

The analysis of the reduced one-dimensional model of figure 9 is now completed by the evaluation of the work expended by the horizontal connector. For the first stretching cycle, this immediately follows from the equations (4.7)–(4.17), namely

$$W^1 = \frac{F_{\text{p}}^2}{k} + 2F_{\text{p}}\left(\tilde{s} - 3\frac{F_{\text{p}}}{k}\right), \tag{4.20}$$

and consists of a term of elastic energy stored in the bristles (first term) and a term of frictional dissipation (second term). Similarly, the work expended by the connector can also be computed for the following cycles, leading to

$$W^n = 2F_{\text{p}}\left(\tilde{s} - 4\frac{F_{\text{p}}}{k}\right), \tag{4.21}$$

an expression comprising only a frictional dissipation term and holding for $n \geq 2$. It is now worth noting that the expressions for the expended work only depend, at fixed gait, on the value of F_{p} and on the ratio of F_{p}/k. As already discussed, kinematic arguments dictate the value of $F_{\text{p}}/k = 0.95$ mm, so that equating the work expended during five cycles as extracted from the finite-element computations, namely 75 mJ, with the corresponding expression from equations (4.20)–(4.21), i.e. for $n = 5$, a value of $F_{\text{p}} = 0.45$ N is obtained, and in turn $k = 0.48\,\text{N mm}^{-1}$. The value obtained for the effective frictional force F_{p} corresponds to the average force acting on the connector as computed via numerical simulations (figure 7*a*). Furthermore, the value of $k = 0.48\,\text{N mm}^{-1}$ is compatible with the horizontal, elastic stiffness of the flexible bristles as determined through beam theory, so that these values definitely confirm the adequacy of the proposed model in resolving both the kinematics and the energetics of the crawler being investigated.

5. Conclusion and perspectives

In this study, a model crawler capable to extract net positional changes from reciprocal, breathing-like deformations was extensively analysed. This remarkable ability of the system relies on directional frictional interactions with a textured substrate, mediated by flexible inclined appendices. Both direct experimentation and nonlinear finite-element computations were exploited to extract the key features of the system, and a reduced, effective model was derived that well captures both the kinematics and the energetics of the crawler gait.

This simplified model provides us with a simple, yet powerful tool for the design and performance prediction of self-propelled robotic crawlers exploiting directional frictional interactions for locomotion.

Future work will consist of the study of the impact of the number and inclination of the bristles on the motility of the crawler. Moreover, different and more generic substrates will be considered, with the anticipation that smoother textures will produce less pronounced oscillations in the mechanical interactions, with smaller discrepancy between peak and average values of the interaction forces.

Finally, we plan to explore the possibility of actually implementing the concepts explored in this study in practical designs of smaller size by exploiting active materials such as liquid crystal elastomers [34,35].

Acknowledgements. We gratefully acknowledge support by SISSA through the excellence programme NOFYSAS 2012 and by the European Research Council through the ERC advanced grant 340685-MicroMotility.

References

1. Childress S, Hosoi A, Schultz WW, Wang J. 2012 *Natural locomotion in fluids and on surfaces: swimming, flying, and sliding*. The IMA Volumes in Mathematics and its Applications, no. 155. New York, NY: Springer.
2. McNeil Alexander R. 2003 *Principles of animal locomotion*. Princeton, NJ: Princeton University Press.
3. Hirose S. 1993 *Biologically inspired robots: snake-like locomotors and manipulators*. Oxford, UK: Oxford University Press.
4. Dreyfus R, Baudry J, Roper ML, Fermigier M, Stone HA, Bibette J. 2005 Microscopic artificial swimmers. *Nature* **437**, 862–865. (doi:10.1038/nature04090)
5. Fletcher DA, Theriot JA. 2004 An introduction to cell motility for the physical scientist. *Phys. Biol.* **1**, 1–10. (doi:10.1088/1478-3967/1/1/T01)
6. Alberts B, Johnson A, Lewis J, Raff M, Roberts K, Walter P. 2002 *Molecular biology of the cell*. New York, NY: Garland Science.
7. Pollard TD, Earnshaw WC. 2008 *Cell biology*. New York, NY: Saunders.
8. Menciassi A, Accoto D, Gorini S, Dario P. 2006 Development of a biomimetic miniature robotic crawler. *Auton. Robot* **21**, 155–163. (doi:10.1007/s10514-006-7846-9)
9. Tanaka Y, Ito K, Nakagaki T, Kobayashi R. 2012 Mechanics of peristaltic locomotion and role of anchoring. *J. R. Soc. Interface* **9**, 222–233. (doi:10.1098/rsif.2011.0339)
10. Guo ZV, Mahadevan L. 2008 Limbless undulatory propulsion on land. *Proc. Natl Acad. Sci. USA* **105**, 3179–3184. (doi:10.1073/pnas.0705442105)
11. Hu DL, Nirody J, Scott T, Shelley MJ. 2009 The mechanics of slithering locomotion. *Proc. Natl Acad. Sci. USA* **106**, 10 081–10 085 (doi:10.1073/pnas.0812533106)
12. Maladen RD, Ding Y, Umbanhowar PB, Kamor A, Goldman DI. 2011 Mechanical models of sandfish locomotion reveal principles of high performance subsurface sand-swimming. *J. R. Soc. Interface* **8**, 1332–1345. (doi:10.1098/rsif.2010.0678)
13. Purcell EM. 1977 Life at low Reynolds number. *Am. J. Phys.* **45**, 3–11. (doi:10.1119/1.10903)
14. Alouges F, DeSimone A, Lefebvre A. 2008 Optimal strokes for low Reynolds number swimmers: an example. *J. Nonlinear Sci.* **18**, 277–302. (doi:10.1007/s00332-007-9013-7)
15. Alouges F, DeSimone A, Lefebvre A. 2009 Optimal strokes for axisymmetric microswimmers. *Eur. Phys. J. E* **28**, 279–284. (doi:10.1140/epje/i2008-10406-4)
16. Alouges F, DeSimone A, Heltai L, Lefebvre A, Merlet B. 2013 Optimal swimming of Stokesian robots. *Discrete Contin. Dyn. Syst. B* **18**, 1189–1215. (doi:10.3934/dcdsb.2013.18.1189)

17. Alouges F, DeSimone A, Giraldi L, Zoppello M. 2013 Self-propulsion of slender micro-swimmers by curvature control: N-link swimmers. *Int. J. Nonlinear Mech.* **56**, 132–141. (doi:10.1016/j.ijnonlinmec.2013.04.012)
18. Arroyo M, Heltai L, Millán D, DeSimone A. 2012 Reverse engineering the euglenoid movement. *Proc. Natl Acad. Sci. USA* **109**, 17 874–17 879. (doi:10.1073/pnas.1213977109)
19. Arroyo M, DeSimone A. 2014 Shape control of active surfaces inspired by the movement of euglenids. *J. Mech. Phys. Solids* **62**, 99–112. (doi:10.1016/j.jmps.2013.09.017)
20. Shapere A, Wilczek F. 1989 Geometry of self-propulsion at low Reynolds number. *J. Fluid Mech.* **198**, 557–585. (doi:10.1017/S002211208900025X)
21. DeSimone A, Tatone A. 2012 Crawling motility through the analysis of model locomotors: two case studies. *Eur. Phys. J. E* **35**, 85. (doi:10.1140/epje/i2012-12085-x)
22. DeSimone A, Guarnieri F, Noselli G, Tatone A. 2013 Crawlers in viscous environments: linear vs non-linear rheology. *Int. J. Nonlinear Mech.* **56**, 142–147. (doi:10.1016/j.ijnonlinmec.2013.02.007)
23. Noselli G, DeSimone A, Tatone A. 2013 Discrete one-dimensional crawlers on viscous substrates: achievable net displacements and their energy cost. *Mech. Res. Commun.* **58**, 73–81. (doi:10.1016/j.mechrescom.2013.10.023)
24. Mahadevan L, Daniel S, Chaudhury MK. 2004 Biomimetic ratcheting motion of a soft, slender, sessile gel. *Proc. Natl Acad. Sci. USA* **101**, 23–26. (doi:10.1073/pnas.2637051100)
25. Hancock MJ, Sekeroglu K, Demirel MC. 2012 Bioinspired directional surfaces for adhesion, wetting, and transport. *Adv. Funct. Mater.* **22**, 2223–2234. (doi:10.1002/adfm.201103017)
26. Gidoni P, Noselli G, DeSimone A. 2014 Crawling on directional surfaces. *Int. J. Nonlinear Mech.* **61**, 65–73. (doi:10.1016/j.ijnonlinmec.2014.01.012)
27. Yoshida R, Takahashi T, Yamaguchi T, Ichijo H. 1996 Self-oscillating gel. *J. Am. Chem. Soc.* **118**, 5134–5135. (doi:10.1021/ja9602511)
28. Maeda S, Hara Y, Sakai T, Yoshida R, Hashimoto S. 2007 Self-walking gel. *Adv. Mater.* **19**, 3480–3484. (doi:10.1002/adma.200700625)
29. Yoshida R. 2010 Self-oscillating gels driven by the Belousov–Zhabotinsky reaction as novel smart materials. *Adv. Mater.* **22**, 3463–3483. (doi:10.1002/adma.200904075)
30. Giomi L, Hawley-Weld N, Mahadevan L. 2013 Swarming, swirling and stasis in sequestered bristle-bots. *Proc. R. Soc. A* **469**, 20120637. (doi:10.1098/rspa.2012.0637)
31. Lubliner J. 1990 *Plasticity theory*. New York, NY: Macmillan Publishing Company.
32. DeSimone A, Grunewald N, Otto F. 2007 A new model for contact angle hysteresis. *Netw. Heterog. Media* **2**, 211–225. (doi:10.3934/nhm.2007.2.211)
33. Fedeli L, Turco A, DeSimone A. 2011 Metastable equilibria of capillary drops on solid surfaces: a phase field approach. *Continuum Mech. Thermodyn.* **23**, 453–471. (doi:10.1007/s00161-011-0189-6)
34. Fukunaga A, Urayama K, Takigawa T, DeSimone A, Teresi L. 2008 Dynamics of electro-opto-mechanical effects in swollen nematic elastomers. *Macromolecules* **41**, 9389–9396. (doi:10.1021/ma801639j)
35. Sawa Y, Urayama K, Takigawa T, DeSimone A, Teresi L. 2010 Thermally driven giant bending of LCE films with hybrid alignment. *Macromolecules* **43**, 4362–4369. (doi:10.1021/ma1003979)